Advanced Structured Materials

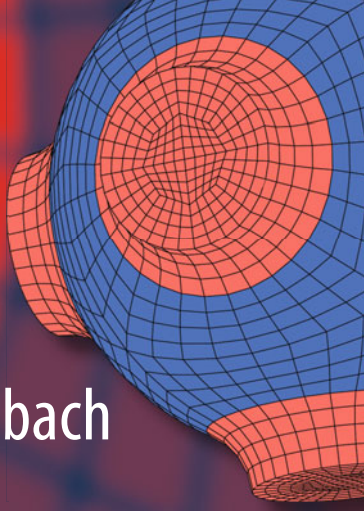

Andreas Öchsner · Holm Altenbach
Editors

Engineering Design Applications

Springer

Advanced Structured Materials

Volume 92

Common engineering materials reach in many applications their limits and new developments are required to fulfil increasing demands on engineering materials. The performance of materials can be increased by combining different materials to achieve better properties than a single constituent or by shaping the material or constituents in a specific structure. The interaction between material and structure may arise on different length scales, such as micro-, meso- or macroscale, and offers possible applications in quite diverse fields.

This book series addresses the fundamental relationship between materials and their structure on the overall properties (e.g. mechanical, thermal, chemical or magnetic etc.) and applications.

The topics of *Advanced Structured Materials* include but are not limited to

- classical fibre-reinforced composites (e.g. class, carbon or Aramid reinforced plastics)
- metal matrix composites (MMCs)
- micro porous composites
- micro channel materials
- multilayered materials
- cellular materials (e.g. metallic or polymer foams, sponges, hollow sphere structures)
- porous materials
- truss structures
- nanocomposite materials
- biomaterials
- nano porous metals
- concrete
- coated materials
- smart materials

Advanced Structures Material is indexed in Google Scholar and Scopus.

More information about this series at http://www.springer.com/series/8611

Andreas Öchsner · Holm Altenbach
Editors

Engineering Design Applications

Springer

Editors
Andreas Öchsner
Faculty of Mechanical Engineering
Esslingen University of Applied Sciences
Esslingen am Neckar
Germany

Holm Altenbach
Lehrstuhl für Technische Mechanik,
Institut für Mechanik, Fakultät für
Maschinenbau
Otto-von-Guericke-Universität
Magdeburg
Germany

ISSN 1869-8433 ISSN 1869-8441 (electronic)
Advanced Structured Materials
ISBN 978-3-319-79004-6 ISBN 978-3-319-79005-3 (eBook)
https://doi.org/10.1007/978-3-319-79005-3

Library of Congress Control Number: 2018936656

Printed on acid-free paper

This Springer imprint is published by the registered company Springer International Publishing AG
part of Springer Nature
The registered company address is: Gewerbestrasse 11, 6330 Cham, Switzerland

Preface

Different engineering disciplines such as mechanical, materials, computer and process engineering provide the foundation for the design and development of improved structures, materials and processes. The modern design cycle is characterized by an interaction of different disciplines and a strong shift to computer-based approaches where only a few experiments are performed for verification purposes. A major driver for this development is the increased demand for cost reduction, which is also connected to environmental demands. In the transportation industry (e.g. automotive or aerospace), this is connected with the demand for higher fuel efficiency, which is related to the operational costs and the lower harm for the environment. One way to fulfil such requirements is lighter structures and/or improved processes for energy conversion. Another emerging area is the interaction of classical engineering with the health and medical sector. This volume gives an overview on recent developments in the mentioned areas of modern engineering design application.

We would like to express our sincere appreciation to the representatives of Springer, in particular to Dr. Christoph Baumann, Senior Editor Engineering, who made this volume possible.

Esslingen am Neckar, Germany — Prof. Dr.-Ing. Andreas Öchsner, D.Sc.
Magdeburg, Germany — Prof. Dr.-Ing. habil. Dr. h. c. mult. Holm Altenbach

Contents

A Remedy for a Family of Dissipative, Unconditionally Stable Explicit Integration Methods

Shuenn-Yih Chang and Chiu-Li Huang

Abstract A family of dissipative structure-dependent integration methods has been developed for structural dynamics. In general, this family of methods can integrate favorable numerical properties together, such as the unconditional stability, explicit formulation, second-order accuracy and controllable numerical damping. Due to the unconditional stability and explicit formulation, it is very computationally efficient for solving general structural dynamics problems. However, an adverse high-frequency overshooting behavior in the steady-state response might be generally experienced if this family of methods is applied to carry out the time integration. The cause of this overshoot is explored. It seems that the incomplete formulation of the difference equation for the displacement increment is responsible for this overshoot. Consequently, this overshooting can be completely eliminated after adding an appropriate load-dependent term into the difference equation for the displacement increment.

Keywords High-frequency overshoot · Steady-state response · Unconditional stability · Explicit formulation · Time integration method · Dynamic analysis

1 Introduction

Structure-dependent integration methods are a new type of time integration methods. It is well known that the coefficients of the two difference equations are generally scalar constants for conventional integration methods while they will become functions of the initial structural properties and the step size for structure-dependent integration methods. The first structure-dependent integration method was developed by Chang in 2002 and it can simultaneously have the unconditional stability

S.-Y. Chang (✉)
National Taipei University of Technology, Taipei, Taiwan, ROC
e-mail: changsy@ntut.edu.tw

C.-L. Huang
Fu Jen Catholic University, New Taipei City, Taiwan, ROC
e-mail: 003951@mail.fju.edu.tw

A. Öchsner and H. Altenbach (eds.), *Engineering Design Applications*,
Advanced Structured Materials 92, https://doi.org/10.1007/978-3-319-79005-3_1

and explicit formulation together [1]. Some other structure-dependent integration methods were proposed to improve numerical properties later [2–8]. Recently, some dissipative structure-dependent integration methods were successfully developed by using an asymptotic equation of motion [9–13]. All of the family methods were enhanced with desirable high-frequency numerical damping. One of them is a free parameter controlled family method [9]. In fact, the parameter p is applied to govern the numerical properties. This family method is referred as Chang dissipative method and will be abbreviated as CDM for brevity herein.

In general, CDM is performed very well in the general dynamic analysis and it is computationally efficient in the step-by-step solution of a nonlinear structural dynamic problem, where the total response is dominated by the low frequency modes while the high frequency responses are of no interest. However, it might experience a new type of overshoot in the steady-state response of a high frequency mode rather than in the early transient response. Notice that an overshoot in the early transient response has been found by Goudreau and Taylor in 1972 [14]. Clearly, the overshoot in this study is different from that found by Goudreau and Taylor since it only occurs under dynamic loading. In this work, the root cause of this overshoot is thoroughly studied and a load-correction scheme is proposed to overcome the overshoot.

2 Chang Dissipative Integration Method

The general formulation of CDM for a single degree of freedom system can be written as:

$$
\begin{aligned}
& m a_{i+1} + c_0 v_{i+1} + \frac{2p}{p+1} k_{i+1} d_{i+1} - \frac{p-1}{p+1} k_i d_i = \frac{2p}{p+1} f_{i+1} - \frac{p-1}{p+1} f_i \\
& d_{i+1} = \beta_0 d_{i-1} + \beta_1 d_i + \beta_2 (\Delta t) v_i + \beta_3 (\Delta t)^2 a_i \\
& v_{i+1} = v_i + \frac{3p-1}{2(p+1)} (\Delta t) a_i - \frac{p-3}{2(p+1)} (\Delta t) a_{i+1}
\end{aligned} \tag{1}
$$

where the coefficients β_0 to β_3 are found to be:

$$
\begin{aligned}
\beta_0 &= -\frac{1}{D}\left[\frac{p-1}{8}\left(\frac{2}{p+1}\right)^3 \Omega_0^2\right] \\
\beta_1 &= 1 + \frac{1}{D}\left[\frac{p-1}{8}\left(\frac{2}{p+1}\right)^3 \Omega_0^2\right] \\
\beta_2 &= \frac{1}{D}\left(1 - \frac{p-3}{p+1}\xi\Omega_0\right) \\
\beta_3 &= \frac{1}{D}\left\{\tfrac{1}{2} - \tfrac{1}{2}\left[\left(\frac{2}{p+1}\right)^2 + \frac{p-3}{p+1}\right]\xi\Omega_0\right\}
\end{aligned} \tag{2}
$$

where ξ is a viscous damping ratio; $\Omega_0 = \omega_0 (\Delta t)$ and $\omega_0 = \sqrt{k_0/m}$ is the natural frequency of the system determined from the initial stiffness k_0.

3 Overshoot Behavior

To illustrate that an unusual overshoot may occur in the steady-state response of a high frequency mode for CDM, the following equation of motion is solved.

$$\ddot{u} + \omega_0^2 u = \varepsilon \omega_0^2 \sin(\bar{\omega} t) \tag{3}$$

where $\bar{\omega}$ is a driving frequency; and ε is a constant for adjusting the response amplitude. The exact solution of this equation for the initial conditions of $u(0) = u_0$ and $\dot{u}(0) = \dot{u}_0$ can be obtained from the fundamental theory of structural dynamics and is found to be:

$$u(t) = u_0 \cos(\omega_0 t) + \left(\frac{\dot{u}_0}{\omega_0} - \frac{\varepsilon \theta}{1 - \theta^2} \right) \sin(\omega_0 t) + \frac{\varepsilon}{1 - \theta^2} \sin(\bar{\omega} t) \tag{4}$$

where $\theta = \bar{\omega}/\omega_0$ is a frequency ratio; u_0 and $\dot{u}_0$ are the initial displacement and velocity, respectively. There will be no transient response in the total response if the initial conditions are chosen to be $u_0 = 0$ and $\dot{u}_0 = \omega_0 \varepsilon \theta/(1 - \theta^2)$.

Three systems are simulated by taking $\omega_0 = 1$, 100 and 1000 rad/s corresponding to S1, S2 and S3. In addition, the driving frequency $\bar{\omega} = 1.5$ rad/s is assumed for each analysis. This leads to $\theta = 1.5$, 1.5×10^{-2} and 1.5×10^{-3} in correspondence to S1, S2 and S3. To demonstrate the unusual overshoot that might be experienced for CDM, two members of CDM are adopted to calculate the responses. The member of $p = 1$ is referred as CDM1 while that of $p = 0.75$ is referred as CDM2. Notice that CDM1 has no numerical damping while CDM2 can have a desired numerical damping. A time step of $\Delta t = 0.1$ s is adopted for time integration. The calculated results are plotted in Fig. 1. This time step is small enough to accurately integrate the steady-state response since the value of $\Delta t/\bar{T}_0$ is as small as $3/40\,\pi$, where $\bar{T}_0 = 2\pi/\bar{\omega}_0 = 4\pi/3$. It has been shown by Chang that a harmonic loading can be very accurately represented if $\Delta t/\bar{T}_0$ is chosen to be less than 1/12 [15]. In Fig. 1 it is shown that either CDM1 or CDM2 can provide accurate solutions for S1 while an overshoot is found in the results of S2 and S3. In Fig. 1a–c it can be seen that the overshoot becomes more significant as the natural frequency increases; and there is almost no overshoot for a low frequency mode. Similar phenomena are also seen in Fig. 1d–f except for the amount of overshoot. This is because that CDM2 can have a desired numerical damping to suppress or even remove the high frequency mode and thus the results obtained from CDM2 show less significant overshoot for S2 and S3 when compared to CDM1. It is evident that CDM experiences an overshoot in the steady-state response of a high frequency mode.

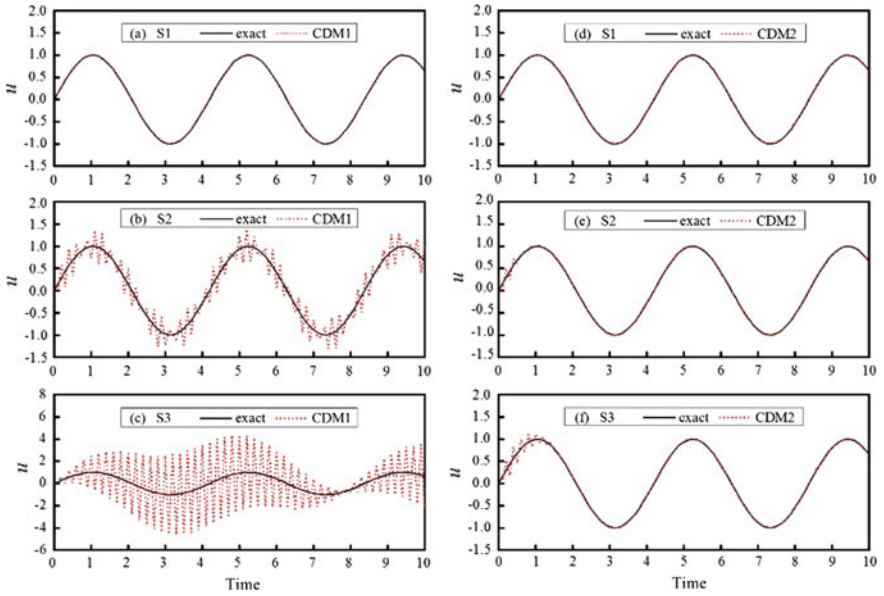

Fig. 1 Forced vibration responses to sine loading for using CDM1 and CDM2

4 Cause of Overshoot

In order to investigate the cause of the overshoot in the steady-state response of a high frequency mode, a local truncation error is constructed from a forced vibration response rather than a free vibration response since the dynamic loading is closely related to the overshoot. A local truncation error is defined as the error committed in each time step by using the differential equation to replace the difference equation. The derivations of the local truncation error for an integration method can be found in the references [1–5] and will not be elaborated herein.

After very complex algebraic manipulations, the local truncation error for CDM for zero viscous damping is found to be:

$$E = \frac{1}{D}\left\{\left[\frac{p(p-2)}{(p+1)^2} + \frac{1}{12}\right](\Delta t)^2 \dddot{u} + \frac{1}{(p+1)^2}\frac{1}{m}(\Delta t)^2 \ddot{f}_i\right\} \tag{5}$$

where

$$D = 1 - \frac{p-3}{p+1}\xi\Omega_0 + \frac{p}{4}\left(\frac{2}{p+1}\right)^3 \Omega_0^2 \tag{6}$$

Clearly, a second-order accuracy can be generally achieved for CDM. It seems that the last error term in Eq. 5 plays the key issue to cause an overshooting phenomenon

in the steady-state response of a high frequency mode for CDM since it can be replaced by the other three terms of the second derivative of the equation of motion:

$$\tfrac{1}{m}\,(\Delta t)^2\,\dddot{f}_i = \Omega_0^2 \ddot{u}_i + 2\xi\Omega_0\,(\Delta t)\,\dddot{u}_i + (\Delta t)^2\,\ddddot{u}_i \tag{7}$$

After substituting this equation into Eq. 5, it will become:

$$E = \frac{1}{D}\left\{\left[\frac{(p-1)^2}{(p+1)^2} + \tfrac{1}{12}\right](\Delta t)^2\,\ddddot{u}_i + \frac{1}{(p+1)^2}\Omega_0^2\ddot{u}_i\right\} \tag{8}$$

In this equation, it is found that the second term is quadratically proportional to Ω_0. Thus, the steady-state response might be almost unaffected by low frequency modes or a small value of Ω_0 while it might be drastically affected by high frequency modes or a large value of Ω_0. Consequently, this local truncation error seems to explain why an overshoot behavior might occur in the steady-state response of a high frequency mode while there is no such overshoot for a low frequency mode.

5 A Proposed Remedy

Since the overshoot in the steady-state response is an adverse behavior for CDM, it is better to eliminate it to obtain an accurate solution. For this purpose, we want to propose a remedy to remove the adverse overshoot behavior in the steady-state response of a high frequency mode. It seems that a slight modification of the formulation of the CDM can be applied to remove the adverse overshoot behavior. Since this modification should not affect the original numerical properties of CDM, a load-dependent term is simply introduced into the difference equation for displacement increments. This is because any load-dependent term will not affect the eigen-analysis of the amplification matrix and thus numerical properties. As a result, the modified form of CDM can be expressed as:

$$\begin{aligned}
&ma_{i+1} + c_0 v_{i+1} + \frac{2p}{p+1}k_{i+1}d_{i+1} - \frac{p-1}{p+1}k_i d_i = \frac{2p}{p+1}f_{i+1} - \frac{p-1}{p+1}f_i \\
&d_{i+1} = \beta_0 d_{i-1} + \beta_1 d_i + \beta_2\,(\Delta t)\,v_i + \beta_3\,(\Delta t)^2\,a_i + q_{i+1} \\
&v_{i+1} = v_i + \frac{3p-1}{2\,(p+1)}\,(\Delta t)\,a_i - \frac{p-3}{2\,(p+1)}\,(\Delta t)\,a_{i+1}
\end{aligned} \tag{9}$$

where q_{i+1} is a load-dependent term. This modified form of the CDM can be referred to as the MCDM herein for brevity. Based on this formulation, the local truncation error for MCDM can be also obtained by using the same procedure to derive that for CDM and it is found to be:

$$E = \frac{1}{D}\left\{\left[\frac{(p-1)^2}{(p+1)^2} + \frac{1}{12}\right](\Delta t)^2 \ddddot{u}_i + \frac{1}{(p+1)^2}\Omega_0^2 \ddot{u}_i\right\} - q_{i+2} + q_{i+1} \tag{10}$$

Apparently, this equation is very similar to Eq. 8, except that the last two error terms are closely related to the load-dependent term, which is intentionally introduced into the difference equation for displacement increments.

In Eq. 10, the load-dependent term q_{i+1} must be properly determined so that the quadratic error term $\Omega_0^2 \ddot{u}_i / D\,(p+1)^2$ in Eq. 8 can be completely removed. After a series of algebraic manipulations, a possible choice of q_{i+1} is found to be:

$$\begin{aligned} q_{i+1} = {} & \frac{1}{D}\frac{1}{(p+1)^2}\frac{1}{m}(\Delta t)^2 (f_{i+1} - f_i) \\ & + \frac{1}{D}\frac{p-1}{(p+1)^3}\frac{1}{m}(\Delta t)^2 (f_{i+1} - 2f_i + f_{i-1}) \end{aligned} \tag{11}$$

Notice that the extra loading term is also structure dependent and the denominator is the same as that for β_0 to β_3. After determining the extra loading term, the local truncation error for CDM is found to be:

$$E = \frac{1}{D}\left[\frac{(p-1)^2}{(p+1)^2} + \frac{1}{12}\right](\Delta t)^2 \ddddot{u}_i \tag{12}$$

It is apparent that the adverse error term as shown in Eq. 8 is no longer in this local truncation error. This strongly indicates that the overshoot in the steady-state response of a high frequency mode is eliminated by the load-dependent term.

6 Numerical Confirmations

In order to verify the effectiveness of the proposed scheme, two numerical examples are examined by using MCDM. Notice that MCDM1 and MCDM2 are in correspondence to CDM1 and CDM2. Apparently, the only difference between CDM and MCDM in the formulation is that the latter has a load-dependent term.

6.1 Example 1

The illustrated example for a forced vibration response of a single degree of freedom system is solved again by using MCDM and the calculated results are plotted in Fig. 2. It is noteworthy that the calculated results obtained from MCDM1 and MCDM2 for a time step of $\Delta t = 0.1$ s are overlapped together with the exact solutions in each plot

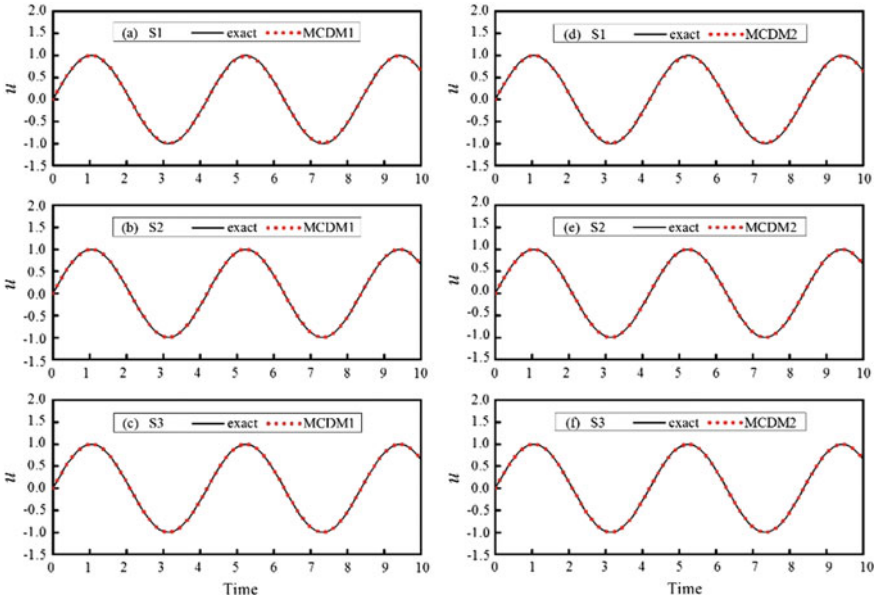

Fig. 2 Forced vibration responses to sine loading for using MCDM1 and MCDM2

of this figure. Thus, it is verified that the proposed scheme can effectively eliminate the adverse overshooting behavior in the steady-state response of a high frequency mode.

6.2 Example 2

In order to show that the adverse overshoot might experience in general dynamic analysis, a 10-story shear-beam type building is used to illustrate that an overshoot in the steady-state response of a high frequency mode may occur in practical applications. The building and its structural properties are shown in Fig. 3, where only a dynamic loading of $10k_1 \sin(3t)$ is intentionally imposed upon the bottom story of the building. The lowest natural frequency of the building is found to be 16.52 rad/s, whereas the highest natural frequency is found to be 10^4 rad/s. Both CDM1 and CDM2 as well as MCDM1 and MCDM2 with a time step of $\Delta t = 0.02$ s are applied to calculate the numerical results. The results obtained from CDM1 and MCDM1 are plotted in Fig. 4. For comparison, the solution obtained from the use of the constant average acceleration method (AAM) with $\Delta t = 0.01$ s is considered as a reference solution.

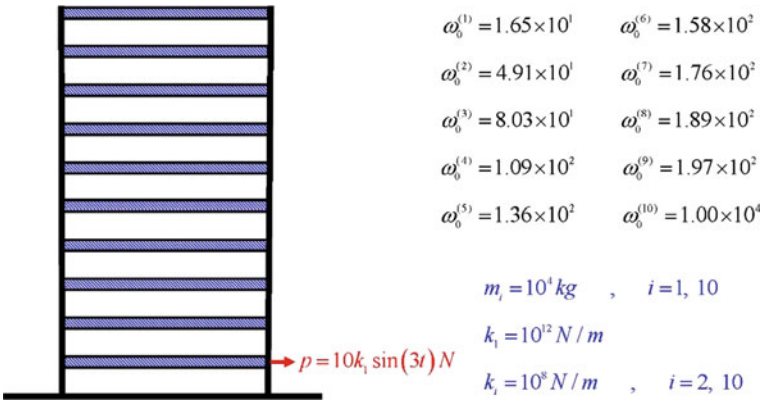

Fig. 3 A 10-story shear-beam type building and its structural properties

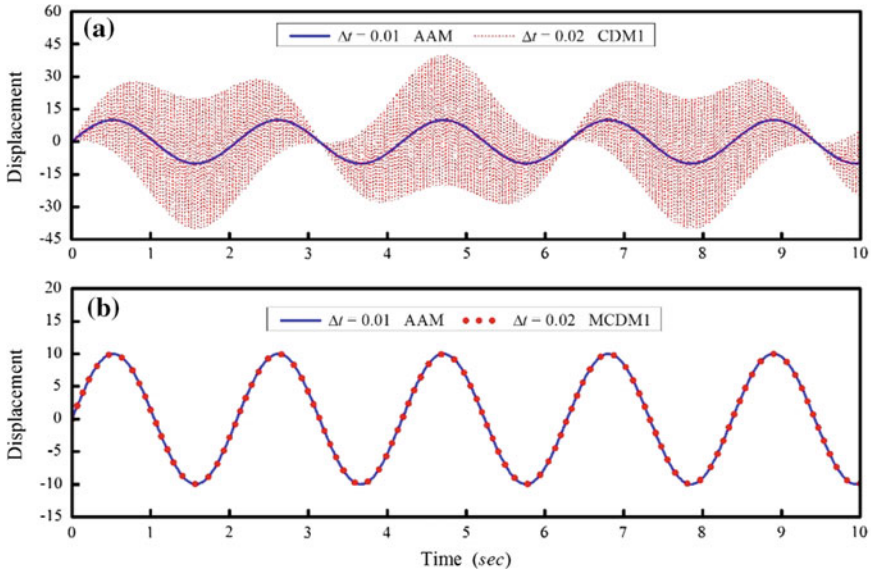

Fig. 4 Forced vibration response to 10-story building at bottom story

As shown in Fig. 4a, the response obtained from CDM1 for the bottom story of the 10-story building exhibits a very significant overshoot behavior. Contrary to this, there is almost no overshoot in Fig. 4b for the responses obtained from MCDM1 since the calculated results are coincided with the reference solutions. Notice that the displacement response at the bottom story is dominated by the steady-state response

since the period of this displacement response is exactly equal to $2\pi/3$ s, which is the period of the sine loading. It is evident from this example that the proposed remedy can effectively remove the adverse overshoot in the steady-state response of a high frequency mode.

7 Conclusions

The one-parameter controlled Chang dissipative structure-dependent family method is very computationally efficient since it can simultaneously integrate the unconditional stability and explicit formulation together. In addition, it also has a second-order accuracy and desired numerical damping. However, it might experience an unusual overshoot in the steady-state response of a high frequency mode. This adverse overshooting can be revealed by the local truncation error constructed from a forced vibration response rather than a free vibration response. In addition, it can be used to derive a remedy to eliminate the adverse overshoot in the steady-state response of a high frequency mode. The remedy is to adjust the difference equation for displacement increment by adding an extra load-dependent term. The effectiveness of this remedy is confirmed by numerical examples in addition to the analytical study. As a result, the additional load-dependent term must be included in the general formulation of the one-parameter controlled Chang dissipative family method so that the adverse overshoot can be automatically eliminated.

References

1. Chang, S.Y.: Explicit pseudodynamic algorithm with unconditional stability. J. Eng. Mech. ASCE **128**(9), 935–947 (2002)
2. Chang, S.Y.: Improved explicit method for structural dynamics. J. Eng. Mech. ASCE **133**(7), 748–760 (2007)
3. Chang, S.Y.: An explicit method with improved stability property. Int. J. Numer. Method Eng. **77**(8), 1100–1120 (2009)
4. Chang, S.Y.: A new family of explicit method for linear structural dynamics. Comput. Struct. **88**(11–12), 755–772 (2010)
5. Chang, S.Y.: Development and validation of a new family of computationally efficient methods for dynamic analysis. J. Earthquake Eng. **19**(6), 847–873 (2015)
6. Chen, C., Ricles, J.M.: Development of direct integration algorithms for structural dynamics using discrete control theory. J. Eng. Mech. ASCE **134**(8), 676–683 (2008)
7. Gui, Y., Wang, J.T., Jin, F., Chen, C., Zhou, M.X.: Development of a family of explicit algorithms for structural dynamics with unconditional stability. Nonlinear Dyn. **77**(4), 1157–1170 (2014)
8. Tang, Y., Lou, M.L.: New unconditionally stable explicit integration algorithm for real-time hybrid testing. J. Eng. Mech. ASCE **143**(7), 04017029-1-15 (2017)
9. Chang, S.Y.: Numerical dissipation for explicit, unconditionally stable time integration methods. Earthquakes Struct. Int. J. **7**(2), 157–176 (2014)
10. Chang, S.Y.: A family of non-iterative integration methods with desired numerical dissipation. Int. J. Numer. Meth. Eng. **100**(1), 62–86 (2014)

11. Chang, S.Y.: Dissipative, non-iterative integration algorithms with unconditional stability for mildly nonlinear structural dynamics. Nonlinear Dyn. **79**(2), 1625–1649 (2015)
12. Chang, S.Y., Tran, N.C., Wu, T.H.: A one-parameter controlled dissipative unconditionally stable explicit algorithm for time history analysis. Sci. Iranica **24**(5), 2307–2319 (2017)
13. Kolay, C., Ricles, J.M.: Development of a family of unconditionally stable explicit direct integration algorithms with controllable numerical energy dissipation. Earthq. Eng. Struct. Dyn. **43**, 1361–1380 (2014)
14. Goudreau, G.L., Taylor, R.L.: Evaluation of numerical integration methods in elasto-dynamics. Comput. Methods Appl. Mech. Eng. **2**, 69–97 (1972)
15. Chang, S.Y.: Accurate representation of external force in time history analysis. J. Eng. Mech. ASCE **132**(1), 34–45 (2006)

Development and Characterization of AA5083 Reinforced with SiC and Al_2O_3 Particles by Friction Stir Processing

Eman M. Zayed, N. S. M. El-Tayeb, M. M. Z. Ahmed and Ragaie M. Rashad

Abstract In this work, friction stir process (FSP) was performed to enhance the surface properties of the aluminum alloy 5083 by incorporating SiC of 6 μm average size, Al_2O_3 of 3 μm average size and mixture of SiC/Al_2O_3 particles in the alloy. Tensile tests, Vickers micro hardness measurements, wear tests, and optical and scanning electron microscopies (SEM) examination were conducted on the surface of Aluminum alloy 5083 to analyze the processed zones of composite samples. Results of tensile tests revealed that ultimate tensile strength of 120 MPa was obtained at 600 rpm. The average hardness increased by 30% with increasing the content of ceramic particles and the maximum hardness values obtained for the hybrid surface composite (50% Al_2O_3 and 50% SiC) developed by 2 passes FSP and processing parameters of 600 rpm. The addition of ceramic powder (SiC) as a reinforcement into AA5083 improved the wear resistance of the received AA5083 by 40%. Hybrid composite of 50% SiC and 50% Al_2O_3 exhibited a superior wear resistance compared to the 100% SiC or 100% Al_2O_3 at a normal load of 20 N.

Keywords Aluminum alloy AA5083 · FSP · Surface modification
Metal matrix composites · Hybrid surface composite

E. M. Zayed (✉) · N. S. M. El-Tayeb · M. M. Z. Ahmed
Mechanical Engineering Department, Faculty of Engineering, The British University in Egypt (BUE), El Shorouk, Egypt
e-mail: eman.zayed@bue.edu.eg

N. S. M. El-Tayeb
e-mail: nabil.eltayeb@bue.edu.eg

M. M. Z. Ahmed
e-mail: mohamed.zaky@bue.edu.eg

M. M. Z. Ahmed
Department of Metallurgical and Materials Engineering, Faculty of Petroleum and Mining Engineering, Suez University, Suez 43721, Egypt

R. M. Rashad
Design and Production Department, Faculty of Engineering, Cairo University, Cairo, Egypt
e-mail: RagaieM.Rashad@bue.edu.eg

A. Öchsner and H. Altenbach (eds.), *Engineering Design Applications*,
Advanced Structured Materials 92, https://doi.org/10.1007/978-3-319-79005-3_2

1 Introduction

Aluminum and its alloys have versatile properties; they are lightweight in addition, their high strength to weight ratio and excellent resistance to corrosion make them suitable for use in structural applications like military, aerospace and transportation industries. However, in some applications, the surface needs to have better mechanical properties such as improved strength and better hardness [1]. Therefore, the reinforcement of surface layer of the component by hard ceramic particles is highly desirable to achieve the required properties while the substrate still maintains the original structure with good ductility and thermal conductivity [2].

In the past, attempts to fabricate metal matrix composites by adding particulate material to the molten alloy followed by casting have not been successful [3]. It has been postulated that the major difficulty in this approach is that the interfacial reaction between reinforcement and metal-matrix cannot be avoided in addition to the formation of some detrimental phases. Therefore, if processing of surface composite is carried out at temperatures below melting point of the substrate, the problems mentioned above can be avoided [4].

Friction stir processing has been evolved as a successful solid state processing technique based on the principle of friction stir welding developed by Mishra [5, 6]. FSP leads to a localized severe plastic deformation of the material and thus can be used for homogenization of microstructure and for grain refinement, thereby resulting in improved material properties. Little or no macroscopic shape change may occur despite the local severity of the plastic deformation [7].

In the view of the above it can be concluded that FSP can be employed to enhance the surface properties (viz. micro-hardness, wear resistance, among others) of metals and their alloys. However, the work pertaining to enhancement of surface properties of aluminum/aluminum alloys through friction stir processing (FSP) is rather scant. In this regard the aim of this study is to investigate the effect of incorporating the surface of AA5083 with micro-sized SiC and Al_2O_3 particles and mixture of them through friction stir processing on its mechanical properties and to study the influence of FSP parameters on the microstructure of the developed metal matrix composite (MMC). In addition to the effect of varying the composition of reinforcement material on mechanical properties (i.e. hardness and tensile) and tribological properties (i.e. wear) were studied with respect to the process parameters.

2 Experimental Procedure

2.1 Material Used

In this study, a cold rolled aluminium alloy (AA5083) plate of 10 mm thickness, 200 mm length, and 50 mm width has been used for the purpose of carrying out FSP. A groove was machined at the center of the substrates with a width of 3 mm and a

Table 1 Nominal chemical composition of 5083 Al alloy (wt%) [8]

	Si	Fe	Cu	Mn	Cr	Mg	Ti	Zn	Al
wt%	0.40 max	0.40 max	0.10 max	0.40/1.0	0.0/0.25	4.0/4.90	0.15 max	0.25 max	Balance

depth of 6 mm. The nominal chemical composition of the alloy 5083 is summarized in Table 1.

The surface of AA5083 is incorporated through FSP with micro-sized SiC and Al_2O_3 powder to produce the (MMC).

2.2 Friction Stir Processing (Equipment)

Figure 1 shows the FSP setup used for carrying the development of MMCs.

A FSP tool of H13 tool steel with shoulder of 25 mm diameter and square probe of 6 mm width and 6 mm length was used to perform the FSP with a schematic shown in Fig. 2, before the start of the actual FSP. The top surface of the grooves was closed using penless tool as shown in Fig. 3a of 25 mm diameter shoulder to prevent the escape of the packed particles during the process and then the FSP was then performed at rotation rate of 400, 600, 800 rpm, constant traverse speed of 60 mm/min, depth of 6 mm, and tool tilt angle was set at 3° with the conventional tool as manifested in Fig. 3b.

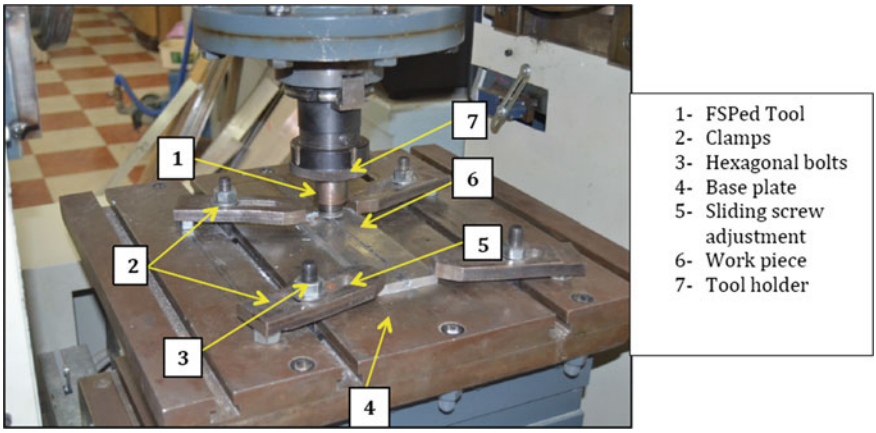

Fig. 1 Clamping arrangement during friction stir processing

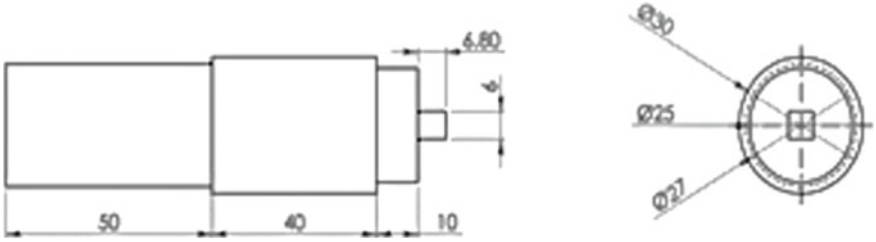

Fig. 2 Schematic illustration of the used FSP tool dimension

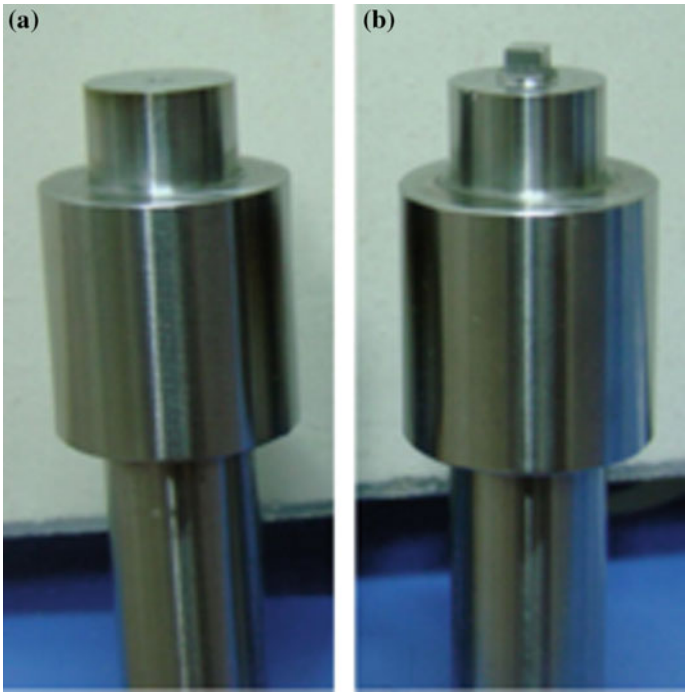

Fig. 3 Friction stir processing tool **a** pinless tool **b** conventional FSP tool

2.3 Metallographic Preparation

Representative sections from the FSPed samples were cut and then were grounded progressively using silicon carbide (SiC) paper, from p60 to p1200 grades, in which each stage progressively removes and replaces the larger surface scratches with smaller ones.

The samples were then polished on 6 and 3 μm diamond cloths for 3–5 min, and finally with an alumina suspension for 5–10 min. Note that after each grinding and polishing step, the samples were washed thoroughly using methanol and air-dried.

2.4 Microstructural Characterization

Optical Microscopy (OM)

The microstructure of the prepared specimens was examined using an optical microscope linked to a high-resolution digital camera. The microstructures were revealed after etching using Keller's reagent.

Scanning Electron Microscope (SEM)

Quanta 250 Field Emission Gun—Scanning Electron Microscope (FEI model: Quanta FEG-250-SEM) was used to examine the reinforcement ceramic particles (SiC and Al_2O_3) and worn surface of the friction stir processed specimens and then they were further analyzed using Energy Dispersive X-Ray Spectroscopy (EDX) within the SEM instrument.

2.5 Mechanical Properties Characterization

To verify the feasibility of using FSP to enhance the mechanical properties of AA 5083, tensile strength and micro-hardness testing at ambient temperature was conducted for FSPed specimens and compared to the As-received AA5083.

Micro-hardness Test

Hardness measurements were carried out on the polished samples. The micro hardness was measured using Vickers hardness tester, the test was carried out at load of 10 HV. The reported results are the average of 10 readings.

Tensile Test

In order to determine the mechanical properties of the materials after FSP, tensile specimens were cut out from the processed zone (PZ) and machined to the specified dimensions according to *ASTM E8* as shown in Fig. 4 of 10 mm and gauge length 50 mm parallel to the processing direction, and tested at room temperature under uniaxial tensile conditions using a universal tensile testing machine. All results were based on the average of three samples from three different processed plates.

2.6 Tribological Characterization

Dry wear behavior of the base metal and surface composite layer (SCL) was studied using a pin on ring tribo-tester. The wear tests were conducted for base material at normal force of 20 N, sliding distance of 800 m and constant track diameter 370 mm. The wear rate is calculated depending on the weights before and after the wear test. The wear behavior of surface composite layer processed after the second pass with

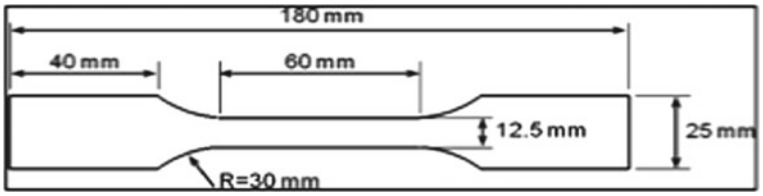

Fig. 4 Schematic diagram showing the dimensions of the tensile specimens used in the uni axial tensile experiment

Fig. 5 Surface appearance of friction stir processed surface at 400 rpm and 100% SiC

additives SiC and Al_2O_3 particles at different FSP conditions were compared with the wear behavior of base material.

3 Results and Discussion

Figures 5 and 6 show the surface appearance of some of the processed surfaces produced at different composition of ceramic particles and rotational speeds. The processed surface showed a considerable amount of flash. A good appearance with a little flash was observed at the lower rotational speed of 400 rpm. The higher flash associated with the higher rotational speed may be attributed to the higher plunging forces applied.

3.1 Microstructural Evolutions

3.1.1 Optical Microstructure

From the micrograph images shown in Fig. 7, it was observed that the agglomeration size of ceramic particles is reduced by increasing number of FSP passes which resulted in improvement of reinforcement particles distribution. Furthermore, pro-

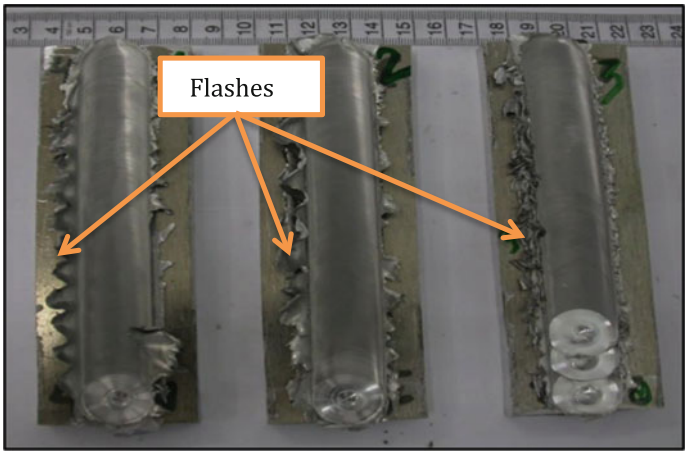

Fig. 6 Surface appearance of friction stir processed surface at 800 rpm and 100% SiC

cessing ceramic particles dispersed more homogenously in the base metal at low rpm, microstructures show that good dispersion areas than with high rpm, since there are voids formed due to low action of homogeneity that resulted from high rotation. This result is in a good agreement with Kwon et al. [9] who studied the FS processed Al 1050 alloy and found the hardness and tensile strength of the FS processed 1050 aluminum alloy were observed to increase significantly with decreased tool rotation speed.

Formation of onion rings is one of the characteristics of FSP, which is found in Fig. 7c.

Figure 7f represents the micro-structure of the hybrid composition of SiC and Al_2O_3 particles at rotational speeds 400 rpm. As shown, clustering of reinforcement particles was observed in Fig. 7f due to the large size of SiC powders, Increasing the number of FSP passes can eliminate this feature.

3.1.2 SEM Microstructure

Figures 8a–f illustrate the SEM micrographs of the nugget cross-sections for processing parameters 400, 600 and 800 rpm for additive composition SiC, Al_2O_3 and mixture of them. Figure 8c shows a uniform distribution of Al_2O_3 powders in the stir zone, Clustering occurs at 800 rpm as shown in Fig. 8f.

Another important note should be mentioned is the alteration of the shape of the nugget with variation of processing parameters. Mishra and Ma [5] represented two types of stirring zone (nugget), basin-shaped nugget and elliptical nugget. For 400 rpm, elliptical-shaped nugget, was observed in Fig. 8e.

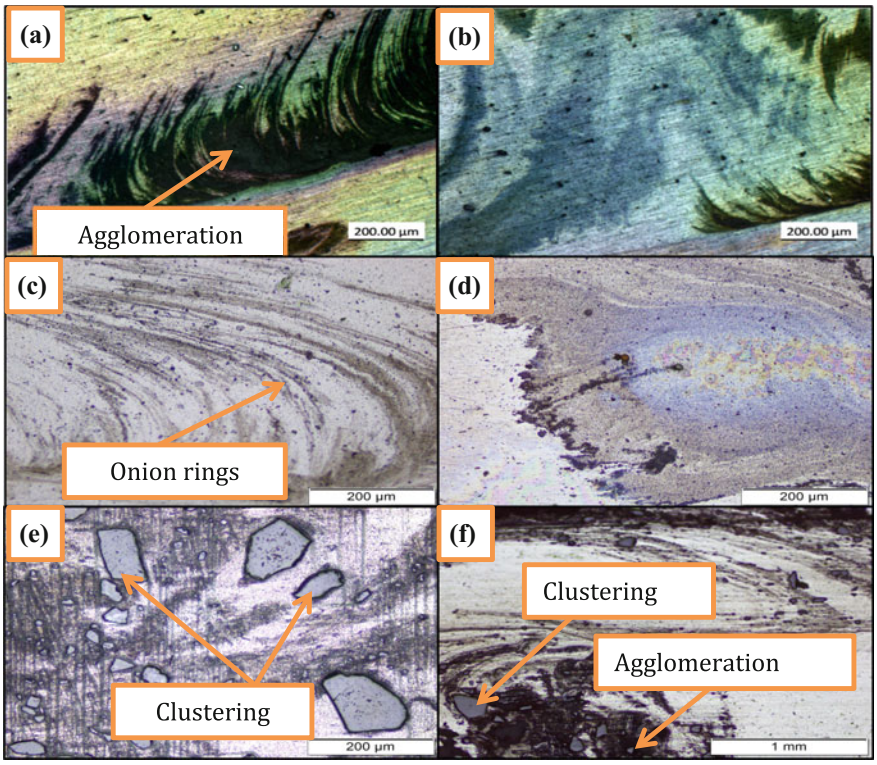

Fig. 7 Optical microscopy images for processed specimens with SiC and Al_2O_3 at different rotational speeds

3.2 Hardness

3.2.1 Effect of Reinforcement Particles Type on Hardness

Micro hardness of friction stir processed specimens was taken using Vickers hardness machine under load of 10 HV. The average hardness values are shown in Table 2 and Fig. 10. It is observed that Vickers hardness values depend on the rotational speeds and this can be interpreted by the frictional heat generated as a result of rubbing of the tool with the matrix. The quantity of frictional heating generated is dependent upon the tool rotation speed. As the tool rotation increases, the amount of frictional heating causing softening and sliding of material during FSP will also increase. Also coarsening of grains due to high heat generated was the main reason for the lowest hardness of those FSPed samples which have been produced at the higher rotation rate compared to the other with lower rotation rate.

It is observed from Fig. 9 that the hybrid surface composites having equal composition (50% SiC and 50% Al_2O_3) exhibit more hardness than the surface composite

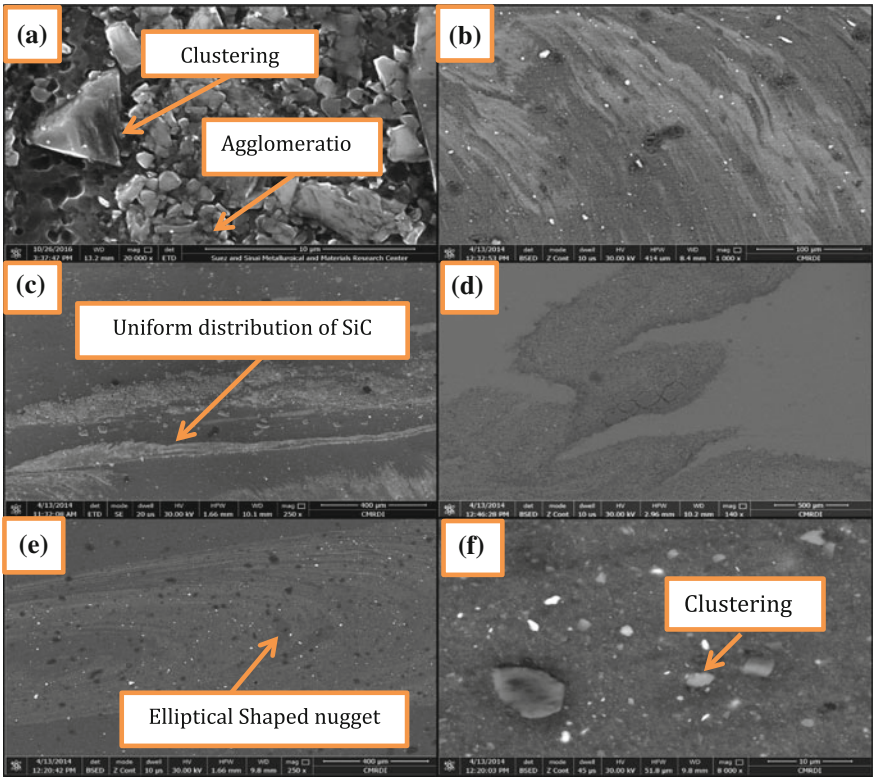

Fig. 8 SEM images for processed specimens with SiC and Al_2O_3 at different rotational speeds

Table 2 Hardness average values

Composition	Rotational speed (rpm)	Hardness avg. (HV)
SiC	400	110.8
	600	106.6
	800	108.4
Al_2O_3	400	101.8
	600	62.34
	800	84.4
SiC and Al_2O_3	400	115.5
	600	117
	800	117

fabricated using other composition of ceramic particles and this result is in a good agreement with Keerthivel et al. [10].

Figures 10 a–c show the micro hardness profile measured across top surface of the FSPed specimens. It is observed that the hardness of processed zone is signifi-

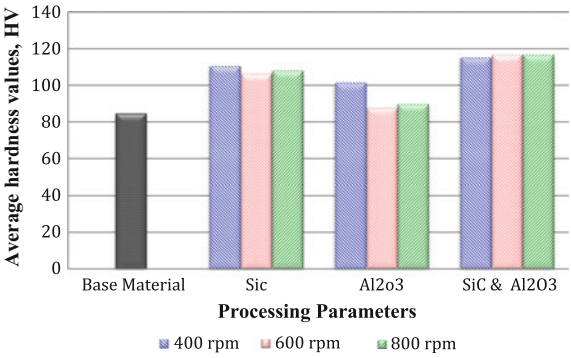

Fig. 9 Effect of the content of ceramic powders and rotational speeds in rpm on the average hardness, HV

cantly higher than that observed for the as-received AA5083 base alloy which has an average hardness of 85 HV. The highest value is observed to be 230 HV for the specimen that underwent 2 passes of FSP at 50% SiC and 50% Al_2O_3. The Vickers hardness value has been characterized as rotational speed dependent [11]. As previously mentioned, the change in rotational and traverse speeds would alter the temperature profile, as well as the exposure time, in the stir zone; this will affect the microstructural characteristics. It can be observed that either increasing the rotational speed and/or changing the type and composition of ceramic powder affect the mechanical properties.

3.3 Evaluation of Tensile Strength

A tensile test of FSPed specimens was carried out. Figure 11 a–c show results of the tensile tests for FSPed specimens with different additive compositions at different rotational speeds. Table 3 shows the ultimate tensile strength (UTS) as well as the 0.2% offset yield values for each FSPed specimen. Two processed specimens were tested for each processing condition and the failure loads were averaged.

The effect of the rotational speed on the ultimate tensile strength of the processed zones is shown in Fig. 12. When the processing is carried out at 600 rpm and with an additive composition of 50% SiC and 50% Al_2O_3, ultimate tensile strength reached to the maximum value of 120 MPa. Conversely by further increasing the rotational speed to 800 rpm, tensile strength slightly decreased again. The reason behind decreasing the UTS values is the incorporation of ceramic particles, which increase the brittleness of the FSPed specimens. However the ductility of the material was greatly improved.